SLURRY EROSION-CORROSION RESISTANCE OF ELECTROLESS Ni-P PLATING ON AISI 5117 STEEL

B. Yosseif Mohamed Saleh

Department of Mechanical Engineering, Assiut University, Assiut, Egypt

Received 13 May 2013, accepted 27 June 2013

ABSTRACT

In this research, slurry erosion-corrosion and slurry-erosion resistances of electroless Ni-P coatings have been investigated. These coatings were applied on AISI 5117 steel discs by electroless deposition process and then they were heat treated at 650˚C for 1 h. Slurry erosion-corrosion and slurry-erosion resistances of deposits were measured by the whirling-arm tester. Also, microstructure of deposits before and after heat treatment was evaluated by X-ray diffraction (XRD) analysis. The results showed that the electroless Ni-P plating greatly increased the erosion and erosion-corrosion resistances for all impact angles. Moreover, the effectiveness of plating was the highest for an impact angle of 45°, where the erosion and erosion-corrosion resistances were increased by 60% and 70% respectively, compared with that of the substrate. The results showed also that the coated and blank specimens behaved as ductile materials under erosion and erosion-corrosion tests and the maximum weight loss occurred at an impact angle of 45°.

Keywords: Slurry erosion-corrosion, Ni-P coating, AISI 5117 steel.

1. Introduction

Considerable economic losses occur every year due to erosion- corrosion in mechanical parts of machines and equipments during service. In order to reduce this loss, properties of the surface of the materials should be improved. One of the methods used to improve the surface quality is surface coating.

Solid particle erosion, a typical wear mode, is material removal/damage to a solid surface produced by repeated impacts of solid particles. It is to be expected whenever hard particles are entrained in a gas or liquid medium impinging on a solid at any significant velocity. The solid-liquid erosion is known as slurry erosion. Slurry erosion has become a serious problem for the performance, reliability, and service life of slurry equipment used in many industrial applications such as: mining machinery components, hydraulic transport of solids in pipelines, marine, oil gas and power generation industries as reported in Refs. [1-6].

The problem of material surface degradation becomes more serious when the liquid-laden particles are corrosive, as in the sea water. By definition, erosion-corrosion is the acceleration in the rate of metal deterioration caused by the combined action of mechanical erosion and electrochemical attack. The joint action of erosion and corrosion is termed erosion-corrosion. This combined effect, often termed synergy, can lead to greater damage and higher metal loss rate beyond that due to either erosion or corrosion alone. The erosion-corrosion is not only responsible for material removal but also leads to premature failure of engineering components. The monetary loss due to erosion-corrosion also includes cost involved in replacement and downtime cost.

* Corresponding author.
E-mail address: bahaa_saleh69@yahoo.com

Slurry erosion is a complex phenomenon and it is not yet fully understood because it is influenced by many factors, which act simultaneously. These factors include flow field parameters, target material properties and erodent particle characteristics. Among these parameters, the impact angle and microstructure of the target material play an important role in the material removal process, based on the data reported in Refs [7-11]. Materials are characterized as either ductile or brittle according to the dependence of their erosion rate on the angle of attack curves [7-9]. For ductile material the erosion rate increases from zero at 0^o impact angle to a maximum when the angle of impact lies between 30^o and 50^o. After reaching the maximum, the erosion rate decreases to a minimum value at 90^o. The effect of impact angle erosion mechanisms of 1017 steel and high-Cr white cast iron using a slurry whirling-arm test rig were investigated [12]. Test results showed that, the effect of impact angle on erosion mechanisms of 1017 steel had three regions. For impact angles $\leq 15^o$, shallow ploughing and particle rolling were the dominant erosion mechanisms. For impact angles lies between 15^o and 75^o microcutting and deep ploughing were observed and for impact angles $\geq 75^o$, indentations and material extrusion prevailed. For high-Cr white cast iron the test results showed that, the erosion mechanisms involved both plastic deformation of the ductile matrix and brittle fracture of the carbides. At low impact angles (up to 45^o) observations of microphotographs of the impacted surfaces revealed that, plastic deformation of the ductile matrix was the dominant erosion mechanism and the carbides fracture was negligible which led to small erosion rate. Whereas, at high impact angles (greater than 45^o) gross fracture and cracking of the carbides were the main erosion mechanisms in addition to indentation with extruded lips of the ductile matrix.

In oil production, the presence of sand combined with various salts and gases results in erosion-corrosion (E-C) of tubing in downstream and upstream conditions [13, 14]. The combined effects of erosion and corrosion can be significantly higher than the sum of the effects of the two processes acting separately. According to a recent survey, erosion-corrosion was rated in the top five most prevalent forms of corrosion damage in the oil and gas production and causes significant economic loss [15]. A number of researches have been conducted to investigate the effects of various operating parameters, such as fluid flow velocity, characteristics of the solid particles, temperature, dissolved oxygen, etc., on E-C of the steel [16-18].

Electroless plating is a chemical reduction process, which depends on the catalytic reduction of a metallic ion from an aqueous solution containing a reducing agent, and the subsequent deposition of the metal without the use of electrical energy. The as-plated electroless nickel deposits has an amorphous phase structure [19]. Subsequent heat-treatment is an important factor that affects the thickness, hardness, structure and morphology of deposit [20]. The electroless deposition is a promising method to prepare durable metal films on both conducting and non-conducting substrates of different geometries. During the past five decades electroless plating has gained popularity due to its ability to offer excellent deposition characteristics, such as uniform coverage, freedom from porosity, hardness, corrosion resistance, solderability, braze and weldability, wear resistance and lubricity [21]. Electroless nickel coatings are the most popular version of electroless coatings which possess some distinct collection of properties [22]. Electroless coatings find their use in almost every domain. From simple knitting needles to the mighty

aerospace applications, their range of applications is continuously broadening. However, studies on the effect of electroless nickel-plate method in resisting slurry erosion are still very limited [23] and not yet widely explored.

In the present work, the slurry erosion-corrosion resistance of low alloy steel (AISI 5117), electroless coated by Nickel-Phosphorus is investigated for different impact angles.

2. Experimental procedures

2.1. Deposition of electroless Ni-P coating

The electroless Ni-P was deposited on AISI 5117 alloy steel flat-surfaced discs of 14 mm in diameter and 10 mm height. The steel nominal composition and mechanical properties are given in Tables 1 and 2, respectively. The substrate flat surfaces were carefully polished with SiC emery papers (from grades No. 80 to No. 4000). All the specimens were subjected to the following pre-treatment and plating procedure:

1- Rinsing by immersion in distilled water at room temperature for 3 min.
2- Ultrasonically cleaned in acetone for 5 min.
3- Rinsing by immersion in distilled water at room temperature for 3 min.
4- Alkaline cleaning in 40% NaOH for 30 sec.
5- Rinsing by immersion in distilled water at room temperature for 3 min.
6-Acid pickling in 10% HCL (MW= 36-46) for 60 sec.
7. Rinsing by immersion in distilled water at room temperature for 3 min.

Table 1
Chemical composition of low alloy steel AISI 5117 [24].

Element	C	Si	Cr	Mn	S	P	Fe
Wt. %	0.17	0.3	0.9	1.2	0.003	0.005	Balance

Table 2
Mechanical properties of low alloy steel AISI 5117 [24].

Yield Strength(MPa)	Tensile Strength (MPa)	Modulus of Elasticity (GPa)	Hardness, Hv (200g)	Density (Kg/m^3)
600	950	210	200	7850

The electroless deposition was carried out in acidic bath. The bath was a glass vessel of 1 L. The chemical constituents for acidic solution bath as well as experimental conditions are presented in Table 3. By using inert metallic wire the samples were hanged in the plating solutions when its temperature reaches 70 °C. Solution stirring is carried out by magnetic stirrer with 110 rpm. After plating is completed (after 60 min) the samples are immediately washed thoroughly by distilled water.

In order to study the film properties, coated samples were thermally treated in a tube furnace under nitrogen. The coatings were isothermally heat treated at 650 °C for 1 h. during heating process, then the samples were allowed to cool down in furnace. The surface morphologies and elemental compositions of the coatings were characterized by

optical microscope and X-ray energy dispersive spectrometer. The hardness of coatings and substrate was measured using (Adolph I, Buehler, Inc) Vickers diamond indenter at a load of 100 g for a loading time of 20 s. The average of five repeated measurements is reported.

Table 3
Electroless nickel phosphorus plating with acidic solution

Chemical Name	Formula	Function	Amount, g/L
Nickel Sulfate	$NiSO_4$- $6H_2O$	Nickel source	15
Sodium hypophosphite	NaH_2PO_2	Reducing agent	26
Sodium acetate	$CH_3COONa \cdot 3H_2O$	Adjusting pH	13
Temp		80-90 °C	
pH		5	

2.2. Experimental procedure

The slurry erosion-corrosion and slurry erosion tests were carried out in a slurry whirling arm rig, which is shown schematically in Fig.1. In whirling test rig, the wear specimens were rotated in a vacuum chamber and a jet of solid liquid falls on the specimen due to gravity flow. The rig is composed of a specimen rotation unit, a slurry unit, and a vacuum unit. Full description of this rig and how it works as well as its dynamics are found in Refs. [25-28]. In this test rig two specimens were clamped in specimen fixtures mounted on two horizontal arms rotated by a variable speed electric motor. The effective rotation diameter of the whirling arms is 248 mm. The specimen fixtures have tilting and locking facilities to adjust the required inclination of the test specimen. The specimen rotation unit provides impact velocity. During slurry erosion tests, only the front surface of specimen is exposed to the impinging slurry since the sides of the specimen are held by the specimen fixture. The front surfaces of the specimens, test surfaces, were 23mm ×10 mm.The impact angle can be adjusted to any required value by rotating the specimen holder around its horizontal axis, as shown in Fig. 2. This assembly is kept in a vacuum chamber as shown in Fig. 1.

The slurry in the chamber falls freely under gravity from a barrel of 25 L capacity, where a stirrer is used to keep the solid-liquid under suspension. The erosion-corrosion tests were carried out in corrosive slurry containing 1 wt. % silica sand and 3 wt. % NaCl aqueous solution. For comparison, slurry erosion tests were conducted under the same particle concentration free from NaCl and the weight loss rate in the water slurry was referred to as erosion rate. The test specimens were cleaned in acetone and then weighed for weight loss using electric balance with an accuracy of 0.1 mg. The velocity of falling slurry stream from the 3 mm diameter funnel orifice is 1.67 m/s, at the specimen surface, impacting every specimen at any pre-set angle between 0 and 90 deg. The impact angle (θ) and impact velocity (v) are correlated to ensure the intended value, which can be obtained from the velocity vector diagram of particle impact, as shown in Fig. 2. In these series of tests, the impact velocity of slurry stream was 15 m/s. The distance between the funnel orifice and the specimen surface is 40 mm. The slurry test chamber is evacuated by a vacuum system (up to 28 cm Hg) to minimize aerodynamic effects on slurry system.

Natural silica sand sieved to a nominal size range of 250 - 355 µm was used as an erodent. A scanning electron microscope (SEM) photograph of typical sand particles is shown in Fig. 3. These particles were characterized using an image analysis method in terms of the aspect ratio (W/L) and roundness factor($P^2/4\pi A$), where W is the particle width, L is the particle length, A is the projected area of the particle, and P is its perimeter. The statistical values of the particle parameters are given in Table 4.

Table 4
Statistical values of particle size and shape as obtained by image analysis of SiO_2 particles

Particle size range (µm)	Statistical parameters	Area A (µm^2)	Average diameter D (µm)	Length L (µm)	Width, W (µm)	Aspect Ratio, W/L	Perimeter P (µm)	$P^2/(4\pi A)$
250-355	Mean	76336.88	301.10	387.08	272.76	0.7180	1117.48	1.36
	Median	76040.1	300.99	375.81	276.32	0.736	1108.79	1.25
	Standard deviation	20507.5	43.60	64.29	44.68	0.14	161.34	0.38

Since the properties of solid particles are of great importance, a single source of erodent particles was used throughout the experiments. Also, fresh particles were used in each test to avoid any degradation of impacting particles during erosion tests.

The difference between the used apparatus in the current study - slurry whirling arm rig - and the other apparatus used in this field is the absence of dependence on time in the present apparatus regarding the comparison among the different impact angles. As shown in Fig. 2, the amount of particles which impacts the surface of specimen per one revolution differs from angle to another. It was found that [25], the mass of particles striking each specimen per one revolution is given by;

$$m_p = \left[l \sin(\theta_0) A_n + \frac{l \cos(\theta_0) Q}{\pi D N} \right] C_w \rho_w \quad (1)$$

Where,

m_p: is the mass of particles striking each specimen per one revolution
l: is the length of wear specimen surface in m
θo: is the angle between the surface plane of the specimen and the horizontal plane.
A_n: is the area of orifice in m^2
Q: is the volume flow rate of slurry in m^3/min., and
D: is the rotational diameter of the wear specimen in m
N: is the rotational speed of the wear specimen in rpm.
C_w: is the weight fraction of solid particles in the water
ρ_w: is the water density in kg / m^3

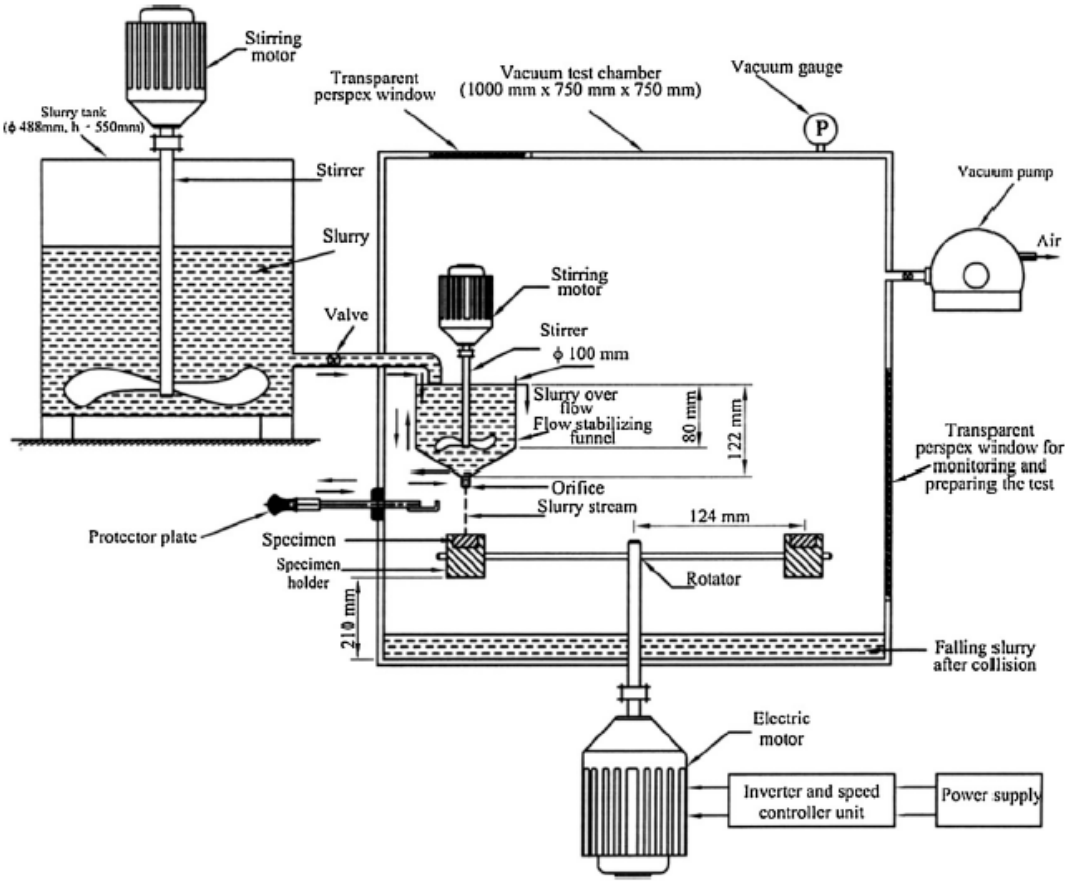

Fig. 1. Schematic diagram of the designed slurry erosion whirling-arm rig.

3. Results and discussion

3.1. Coating surface morphology

Figure 4 shows the optical images of the surface morphologies of Ni-P coating before and after heat treatment. The deposit surface morphology before heat treatment reveals that all the electroless Ni-P deposits were uniformly and continuously covered with precipitates of the electroless Ni-P deposition, and there were no obvious flaws or apertures on the coating surface. As well as, all deposit surfaces are smooth, the smooth coating suggests the better protectiveness of the Ni-P coating. However, the surface morphology after heat treatment showed a discernible changes, where a clear crystalline structure appeared.

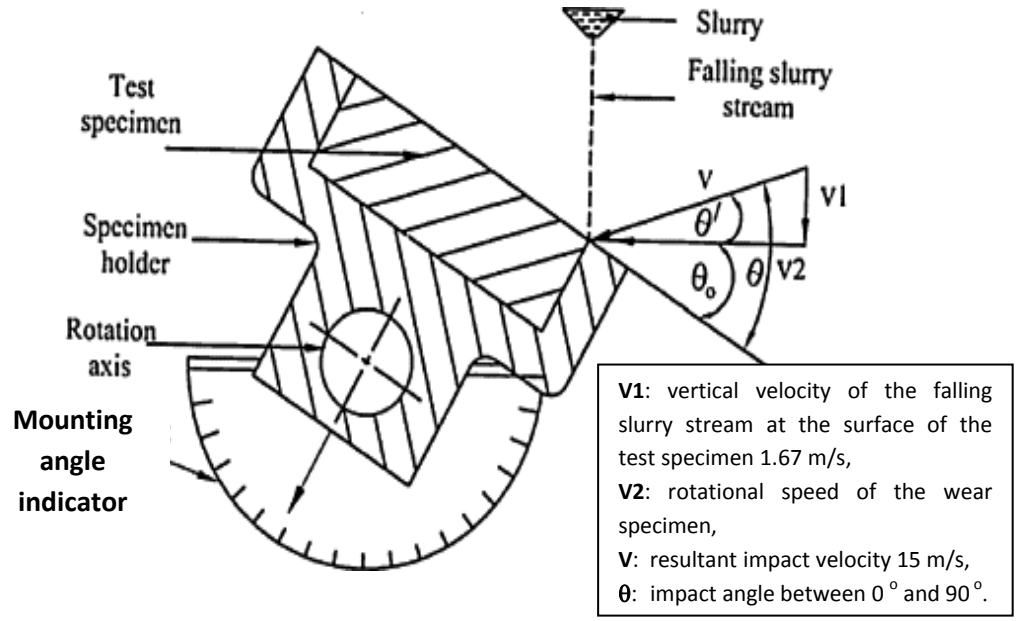

Fig. 2. Schematic diagram of impact velocity and impact angle.

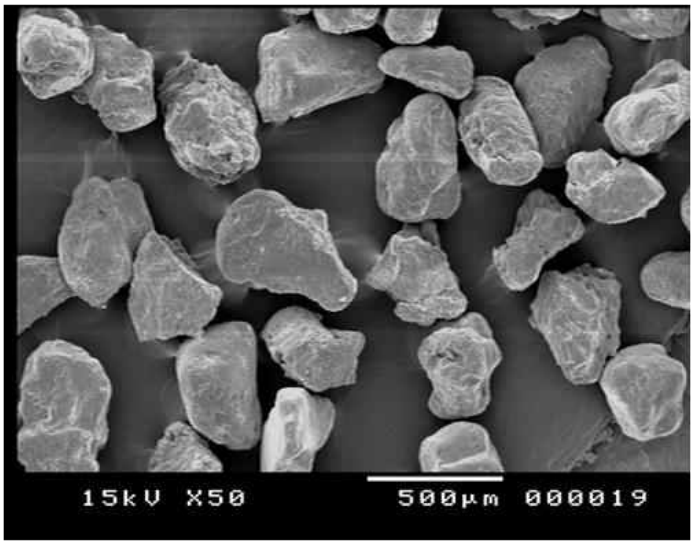

Fig. 3. SEM photograph of silica sand (mean diameter = 302µm).

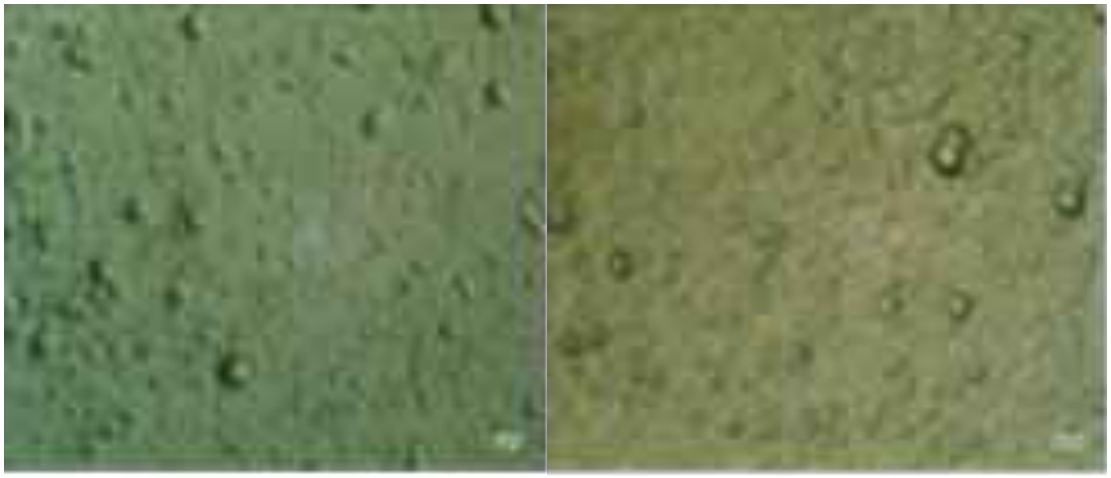

(a) (b)

Fig. 4. Optical micrograph of electroless nickel coated layer, (a) as-deposited and (b) after heat treatment

This has been observed in many works [e.g. 29-31]. Rabizadeh et al. [29] made a scan analysis of Ni-P coating heat treated at 600 °C (for 15 min). Their results showed a formation of an inter-diffusional layer and its elemental distribution that affected the coating properties. They explained the formation of an inter-diffusional layer, as a result of inter-diffusion of nickel and phosphorous from the coating to the substrate and iron in the reverse direction from the substrate would develop upon heating at 600°C. The deposit thickness was determined from optical micrographs of the metallographic cross-section of the electroless coating and is shown in the Fig. 5. The thickness value was in the range of 25-28 µm. Figure 6 shows the X-ray diffraction (XRD) patterns of electroless Ni-P coatings of as plated and post heat treated films. As shown in Fig. 6, the XRD patterns of the as-plated sample before heat treatment revealed a single peak at 45^{o}. When Ni-P deposits were heat-treated for 1 hr at 650 °C, their structures underwent modification as shown in Fig. 6. It can be seen from the XRD patterns that many XRD peaks corresponding to crystalline fcc Ni and Ni_xP_y appeared.

Many researches have shown that heat treatment of the as-deposited coatings caused a transformation from a supersaturated solid solution of phosphorus in nickel to a nickel matrix plus Ni_3P [32]. It has been reported that different heating conditions also have shown significant influences on both the microstructural properties and crystallization behaviors of the electroless nickel deposits [32]. As a result of solid-state diffusion, the structures will revert to the thermodynamically most stable state. The amorphous deposits undergo a crystal growth process, and such heat treatment results in a mixture of relatively coarse-grained metallic nickel together with intermetallic phase.

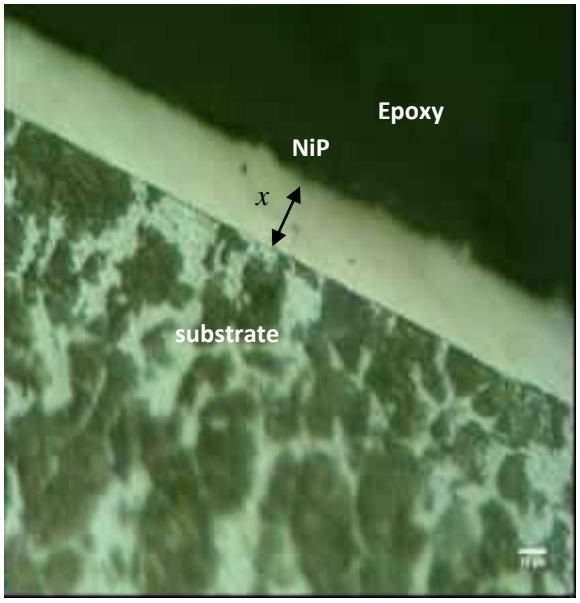

Fig.5. Cross-section SEM micrographs of Ni-P coating, x: thickness of Ni-P deposit.

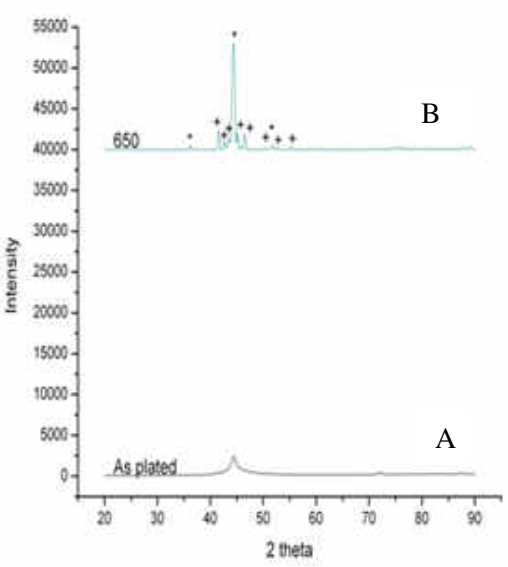

Fig. 6. XRD analysis result of Ni-P coating, A: as-plated, and B: heated at 650 °C for 1 h.

3.2 .Effect of impact angle

Figure 7 shows the relationship between the cumulative mass loss and impact angle for the blank and Ni-P coated specimens for erosion and erosion-corrosion tests. For comparison, the results obtained in tap water slurry are also presented. The mass of erodent was 112.374 gm for all impingement angles. As the corrosion of the specimens in tap water is negligible [3], the mass loss in tap water slurry is referred to as erosion mass loss WE. The mass loss in the sodium chloride slurry is referred to as the erosion-corrosion mass loss WEC. The WEC-curve varies in a similar manner to the WE-curve for blank and coated specimens. The mass loss initially increases and then decreases with impact angles increasing from 15° to 90°, reaching a maximum at about 45°. However, WEC is higher than WE at all impact angles for coated and blank specimens. It is clear from the results that the coating resulted in lower mass losses for corrosive and erosive tests at all impact angles. However, the highest effectiveness for coating is marked at 45°. The highest mass losses are obtained for the blank specimen. The WEC- and WE- curves shown in Fig. 6 show typical ductile erosion behavior, as explained below. For ductile materials, impingement at low impact angles will increase material removal by microcutting and ploughing due to the oblique shear force [33] and thus increase the mass loss. At high impinging angles, the resolved normal stress will produce accumulated damage mainly

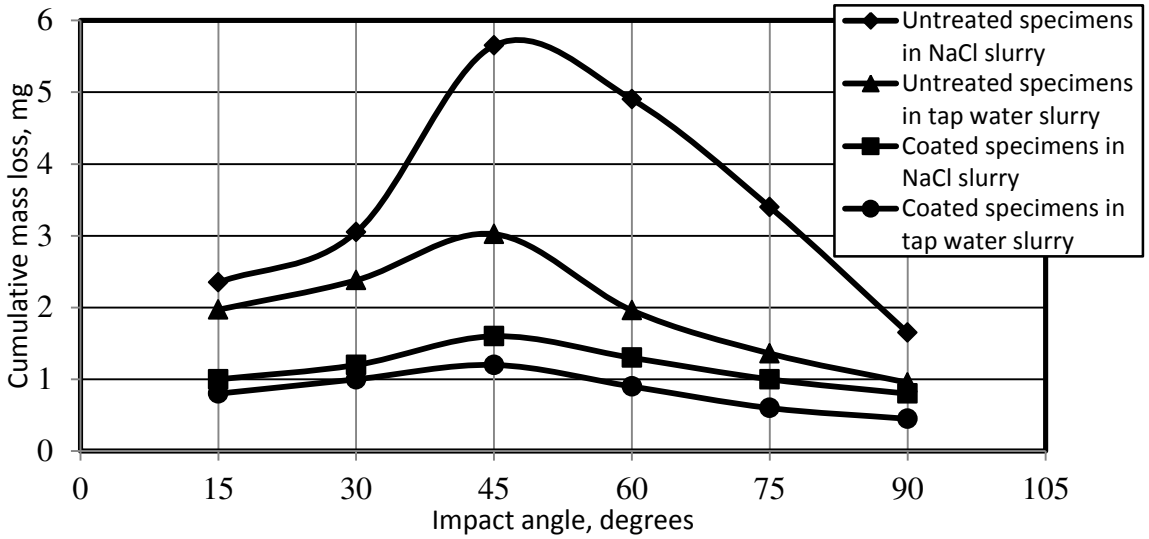

Fig. 7. Relationship between the mass loss of coated and blank specimens and impact angle for tap water slurry and NaCl slurry.

during the microforging and extrusion processes [34]. These processes produce less erosion damage than that produced by cutting removal and ploughing at low impinging angles. Hence, the maximum mass loss appears at an impact angle of approximately 45°.

Therefore, in hydraulic equipment made of low carbon alloy steel, it is recommended to carry out Ni-P coatings for surfaces subjected to slurry erosion especially when the angle of impact is low or intermediate. At normal impact angle the economic factor must be considered.

3.3 .Change of mass loss with time for impact angle of 45°

To highlight the effect of coating on the enhancement of erosion and corrosive resistance, the mass loss variation of coated and blank specimens with test time at an impact angle of 45° is presented in Fig. 8. It is clear from this figure that coating of steel improves the erosion-corrosion resistance and the erosion resistance, but the improvement of the former is the higher. The results at a time of 420 min shown in Figs. 8 and 9 illustrate that the erosion-corrosion and erosion resistance of AISI 5117 steel increases by 70 % and 60 % respectively as a result of coating. As observed in Fig. 8, the WEC and WE are found to increase linearly with increasing erosion time for coated and blank specimens in the tap water slurry and the sodium chloride slurry. This indicates that the erosion mechanism does not change noticeably, implying a steady erosion damage during the impingement processes.

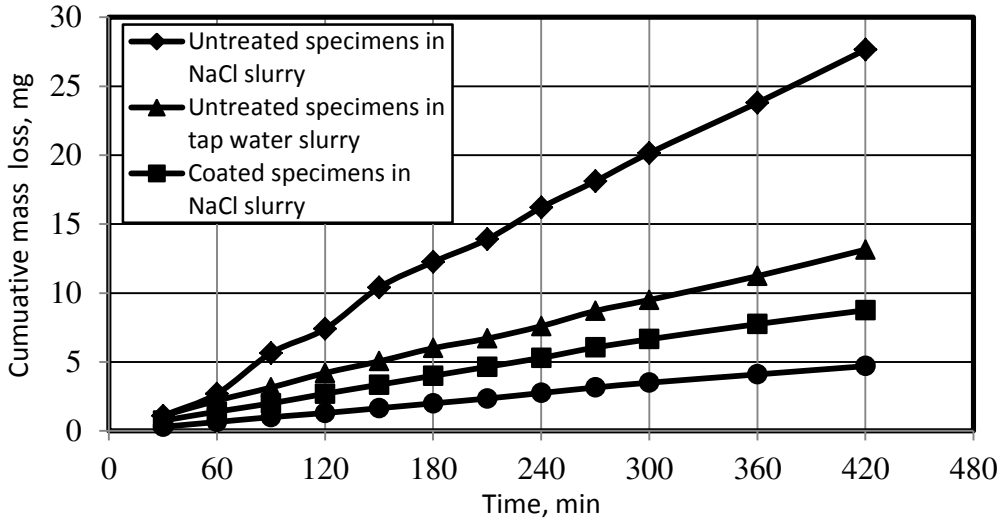

Fig. 8. Mass loss of coated and blank specimens versus test time for tap water slurry and NaCl slurry at impact angle of 45°.

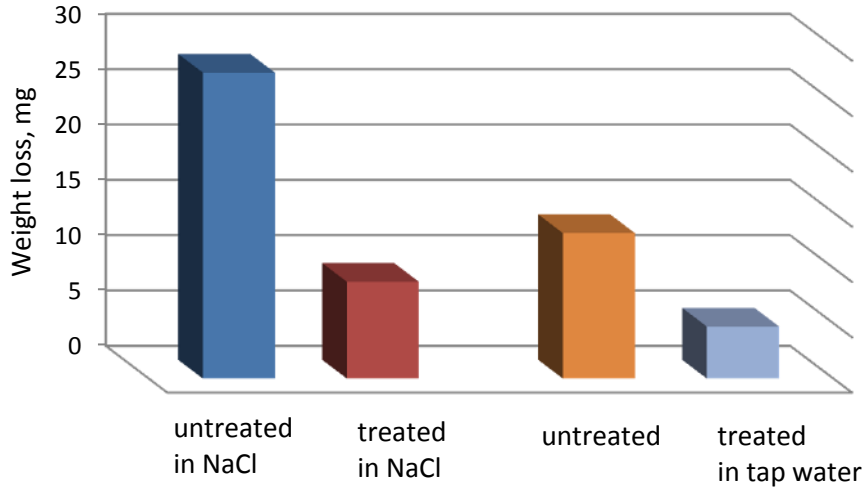

Fig. 9. Mass loss of coated and blank specimens for tap water slurry and NaCl slurry at impact angle of 45° and 420 min test time.

4. Conclusions

The slurry erosion-corrosion and slurry erosion processes, microstructure and thickness of electroless Ni-P deposited on AISI 5117 carbon steel at an acidic bath for 1 h and heat treated at 650 °C were investigated. The obtained results may be summarized as follow.

1. Electroless Ni-P plating of AISI 5117 low carbon alloy steel specimens showed much better slurry erosion-corrosion and slurry-erosion resistances than the blank specimens for all impact angles, but the highest resistance was at an angle of 45°.
2. The maximum mass loss for erosion and erosion-corrosion appears at an impact angle of 45° for coated and blank specimens.
3. Electroless Ni-P plating showed greater resistance to erosion-corrosion than the resistance to erosion.

5. References

[1] Fang, O., Sidky, P.S., and Hocking, M.G., "Microripple Formation and Removal Mechanism of Ceramic Materials by Solid-Liquid Slurry Erosion", Wear, 223, pp. 93-101, 1998.
[2] Lathabai, S., and Pender, D. C., "Microstructure Influence in Slurry Erosion of Ceramics", Wear, 189, pp.122-135, 1995.
[3] Li, Y., Burstein, G.T., and Hutchings, I. M., "The Influence of Corrosion on the Erosion of Aluminum by Aqueous Silica Slurries", Wear, 186-187, pp. 515- 522, 1995.
[4] Iwai, Y., and Nambu, K., "Slurry Wear Properties of Pump Lining Materials", Wear, 210, pp. 211-219, 1997.
[5] Tsai, W., Humphrey, J.A.C., Cornet, I., and Levy, A.V., "Experimental Measurement of Accelerated Erosion in a Slurry Pot Tester" Wear, 68, pp. 289- 303, 1981.
[6] Stanisa, B., and Ivusic, V., "Erosion Behaviour and Mechanisms for Steam Turbine Rotor Blades", Wear, 186-187, pp. 395-400, 1995.
[7] Burstein, G.T., and Sasaki, K., "Effect of Impact Angle on the Slurry Erosion-Corrosion of 304L stainless steel", Wear, 240, pp. 80-94, 2000.
[8] Oka, Y.I., Ohnogi, H., Hosokawa,T., and Matsumura, M., "The Impact Angle Dependence of Erosion Damage Caused by Solid Particle Impact", Wear, 203- 204, pp. 573-579, 1997.
[9] Clark, H.M., and Wong, K.K., "Impact Angle, Particle Energy and Mass loss in Erosion by Dilute Slurries", Wear, 186-187, pp. 454-464, 1995.
[10] Fang,Q., Xu,H., Sidky, P.S., and Hocking, M.G., "Erosion of Ceramics Materials by a Sand/Water Slurry Jet", Wear, 224, pp. 183-193, 1999.
[11] Chen, K.C., He, J.L., Huang, W.H. and Yeh,T.T., "Study on the Solid-Liquid Erosion Resistance of Ion-Nitrided Metal", Wear, 252, pp. 580-585, 2002.
[12] Al-bukhaiti, M.A., Ahmed,S.M., Badran, F.M.F., and Emara, K. M., "Effect of Impact Angle on Slurry Erosion Behavior and Mechanisms of 1017 Steel and High-Chromium White Cast Iron", Wear, 262, pp. 1187-1198, 2007.
[13] Hamzah, R., Stephenson, D.J., and Strutt, J.E., "Erosion of Material Used in Petroleum Production," Wear, 186-187, pp. 493-496, 1995.
[14] Stack, M.M., and Abdulrahman, G., "Mapping Erosion-Corrosion of Carbon Steel in Oil Exploration Conditions: Some New Approaches to Characterizing Mechanisms and Synergies", Tribol. Int., 43 (7), pp. 1268-1277, 2010.
[15] McLintyre, P., "Marine Corrosion" Club Meeting, Aberdeen, April, 1999
[16] Tian, B.R., and Cheng, Y.F., "Electrochemical Corrosion Behavior of X-65 Steel in the Simulated Oil Sand Slurry. I: Effects of Hydrodynamic Condition", Corros. Sci. 50, pp. 773-779, 2008.
[17] Jiang,X. Zheng, Y.G., and Ke, W., "Effect of Flow Velocity and Entrained Sand on Inhibition Performances of Two Inhibitors for CO2 Corrosion of N80 Steel in 3% NaCl Solution" Corros. Sci. 47, pp. 2636-2641, 2005.
[18] Guo, H.X., Lu, B.T., and Luo, J.L., "Interaction of Mechanical and Electrochemical Factors in Erosion-Corrosion of Carbon Steel", Electrochim. Acta, 51, pp. 315-323, 2005.

[19] Ashassi-Sorkhabi, H., and Rafizadeh, S.H., "Effect of Coating Time and Heat Treatment on Structures and Corrosion Characteristics of Electroless Ni-P Alloy Deposits", Surf. Coat Technol., 176 (3), pp. 318-26, 2003.
[20] Apachitei, I., Tichelaar, T.D., Duszczyk, J., and Katgerman, L., "The Effect of Heat Treatment on the Structure and Abrasive Wear Resistance of Autocatalytic NiP and NiP-SiC Coatings", Surf. Coat Technol., 149, pp. 263-278, 2002.
[21 Smith, N.M., "The Fantastic Potential of Elecuoless Nickel", Proceedings of the Elecrroless Nickel Conference, Cincinnati, June 24-28, 1997.
[22] Prasanta Sahoo, and Suman Kalyan Das, "Tribology of Electroless Nickel Coatings - A Review", Materials and Design, 32(4), pp. 1760-1775, 2011.
[23] Ray Taheri, "Evaluation of Electroless Nickel-Phosphorus (EN) Coatings", Ph. D. thesis, University of Saskatchewan, 2003.
[24] Bohler, "Special Steel Manual", A-8605 Kapfenberg, Germany, 90-98, 2000.
[25] Abou-Elkasem,A., Abd-Elrhman,Y.M., Ahmed,S.M. and Emara,K.M., "Design and Performance of Slurry Erosion Tester", ASME J. Tribol., 132 (2), pp. 021601, 2010.
[26] Abou-elkasem, A.," Particle Size Effects on Slurry Erosion of 5117 steels", ASME J.Tribol., 133 (1), pp. 014502, 2011.
[27] Abd-Elrhman,Y.M., Abou-Elkasem,A., Ahmed,S.M. and Emara,K.M., "Effect of Impact Angle on Slurry Erosion Behaviour and Mechanisms of Carburized AISI 5117 Steel", under 2nd revision in Wear.
[28] Abouel-Kasem, A., Ezz El-Deen, A, Ahmed, S. M., "Wear Characteristics of Welding Materials in Slurry", JES, Fac. of Eng., Assiut Univ, Egypt, Vol.33, No. 6 , pp.2165-2177, 2005.
[29] Rabizadeh, T., Allahkaram, S.R. and Zarebidaki,A., "An investigation on effects of heat treatment on corrosion properties of Ni-P electroless nano-coatings, Materials and Design, 31, pp. 3174-3179, 2010.
[30] Krishnamoorthy, P. R., Narayana, B. H., Ramakrishna, T.V., and Shekhar Kumar, M., "Properties of Electroless Nickel-Phosphorus Deposits after Crystallization", Metal Finish, pp. 13-17, 1192.
[31] Guo, Z., Keong, K.G, and Sha, W., "Crystallisation and Phase Transformation Behaviour of Electroless Nickel Phosphorus Plating during Continuous Heating", J. of Alloys and Compounds, 358, pp. 112-119, 2003.
[32] Randin, J.P., Maire, P.A., Saurer, E., and Hintermann, H.E., "DTA and X- ray Studies of Electroless Nickel", J. Electrochemical Soc., 114 (5), pp. 442-445, 1967.
[33] Finnie, I., and McFadden, D.H., "On the Velocity Dependence of the Erosion of Ductile Metals by Solid Particles at Low Angles of Incidence", Wear, 48, pp. 181-190, 1978.
[34] Bellman Jr., R., and Levy, A., "Erosion Mechanism in Ductile Metals", Wear, 70, pp. 1-27, 1981.

مقاومة سبيكة الفولاذ (AISI 5117) المطلية لاكهربائي بالنيكل والفوسفور للتآكل بالنحر المصحوب بالتآكل الكهروكيميائي في الملاط

الملخص العربى

في هذا البحث تمت دراسة مقاومة كلاً من التآكل بالنحر المصحوب بالتآكل الكهروكيميائي والتآكل بالنحر للطلاء اللاكهربائي بالنيكل مع الفسفور. وقد تم ترسيب الطلاء اللاكهربائي على أقراص من سبيكة الفولاذ (AISI 5117) وبعد ذلك تم معالجة تلك الأقراص المطلية لمدة ساعة عند درجة حرارة 650 درجة مئوية. اختبارات التآكل بالنحر والتآكل بالنحر المصحوب بالتآكل الكهروكيميائي أجريت باستخدام جهاز الأذرع الدوارة. وكذلك تم فحص البنية الدقيقة للطلاء قبل وبعد المعالجة الحرارية.
ولقد أظهرت النتائج أن الطلاء اللاكهربائي بالنيكل مع الفسفور يزيد المقاومة لكلا التآكلين لكل زاويا الاصطدام ولكن الفعالية الأكبر للمقاومة كانت عند زاوية 45 درجة حيث زادت المقاومة للتآكل بالنحر والتآكل بالنحر المصحوب بالتآكل الكهروكيميائي بمقدار 60% و70 % على التوالي مقارنة بتلك التي لسبيكة الفولاذ بدون طلاء. وأوضحت النتائج أيضا أن العينات الغفل والعينات المطلية تتصرف التصرف اللدن لكلا التآكلين وأن الفقد الأعظم في المادة كان عند الزاوية 45 درجة.